# Calculating Crystal Field Splitting via maximally localized Wannier functions

Valentina Mazzotti*
*Department of Physics, McGill University, Montreal, Quebec H3A 2T8, Canada*

(Dated: December 25, 2024)

This study presents a method for calculating the crystal field splitting $\Delta_o$ using Maximally Localized Wannier Functions (MLWF) in two cubic perovskites, $SrVO_3$ and $TiPbO_3$. High-quality Wannier functions are constructed, and their accuracy is assessed in terms of their spread and localization. By constructing tailored sets of Wannier functions to include varying levels of hybridization, we analyze trends in crystal field splitting and demonstrate how hybridization with surrounding ligand $p$- and $s$-orbitals contributes significantly to the ligand field splitting. This approach is first applied to $SrVO_3$, a representative transition metal oxide with well-separated $t_{2g}$ and $e_g$ states. The same technique is subsequently extended to $TiPbO_3$, a system which displays a band structure with overlapping groups of bands, lacking the distinct separation between different dominant orbital characters seen in $SrVO_3$.

## I. INTRODUCTION

One of the foundational concepts in the theory of transition metal (TM) oxides is the interaction of a TM ion with the electrostatic potential created by its surrounding ions, known as the crystal field [1]. Crystal field theory predicts that in transition metal oxides, particularly in perovskites, the $d$-orbitals of the TM cation split into two energy levels: the lower-energy $t_{2g}$ orbitals and the higher-energy $e_g$ orbitals, separated by the crystal field splitting energy. This splitting results from the interaction between the $d$-electrons of the TM ion and the electrostatic field generated by surrounding anions, influencing phenomena such as magnetism, Mott insulating behavior, and Jahn-Teller distortions [2]. For the past 30 years, density functional theory (DFT) has been the dominant method for the quantum mechanical simulation of periodic systems, as it provides a computationally efficient approach for studying the electronic structure of atoms, molecules, and solids [3]. While the electronic ground state of a periodic system is often described using extended Bloch orbitals, an alternative representation in terms of localized "Wannier functions" was introduced by Gregory Wannier in 1937 [4]. In this work, we extract the crystal field splitting in the perovskites $SrVO_3$ and $TiPbO_3$ by reconstructing their electronic structures using density functional theory (DFT) combined with maximally localized Wannier functions (MLWFs) [5]. By constructing sets of Wannier functions corresponding to different energy windows, we can successively distinguish between the pure electrostatic contribution and the hybridization components with different ligand states in the derived crystal field splitting. For the first time, the crystal field splitting in $TiPbO_3$ has been calculated *ab initio*, along with a detailed characterization of its hybridization with the surrounding ligands. Unlike systems with well-separated bands, such as $SrVO_3$, $TiPbO_3$ features highly mixed orbital characters, making it significantly more challenging to construct a suitable tight-binding model. The paper is organized as follows: the Theory section (II) introduces the principles of crystal field theory (CFT) and the construction of maximally localized Wannier functions (MLWFs). This is followed by a brief overview of the workflow (III A) used to construct a simplified yet accurate description of the electronic structure, enabling the derivation of the crystal field splitting. Finally, we present the results for the two perovskite oxides, $SrVO_3$ and $TiPbO_3$.

* Email: valentina.mazzotti@mail.mcgill.ca

## II. THEORY

### A. Crystal field splitting in octahedral complexes

Crystal field theory (CFT) describes the breaking of degeneracies of electron orbital states, usually $d$ or $f$ orbitals, due to a static electric field produced by a surrounding charge distribution (the anion neighbors) [6]. As a ligand approaches the metal ion, the electrons from the ligand will be closer to some of the d-orbitals and farther away from others, causing a loss of degeneracy, and giving rise to the characteristic energy splitting of the d-orbitals. This split is influenced by factors such as the metal's oxidation state, ligand geometry and arrangement, the coordination number, and the type of ligands [7]. Consequently, each system has its own crystal field splitting, and precise determination of its value requires either experimental measurements or *ab-initio* calculations specific to the system. The most common type of complex investigated in CFT is octahedral, in which six ligands form the vertices of an octahedron around the metal ion. Taking $SrVO_3$ as an example, the vanadium (V) atom, shown in light blue in Fig. 1, is positioned at the center of an octahedron formed by six surrounding oxygen (O) atoms (red). This octahedral arrangement

of ligands ($O^{2-}$ anions) creates a crystal field that interacts with the $d$-orbitals of the central $V^{4+}$ ion. In this environment, the $d_{xy}$, $d_{xz}$, and $d_{yz}$ orbitals experience less repulsion from the ligands and are therefore lower in energy, collectively referred to as the $t_{2g}$ set. In contrast, the $d_{z^2}$ and $d_{x^2-y^2}$ orbitals, which are oriented directly towards the ligands, experience higher repulsion and form the higher-energy $e_g$ set [2, 8]. The difference in energy between these two sets is what we refer to as crystal field splitting $\Delta_o$.

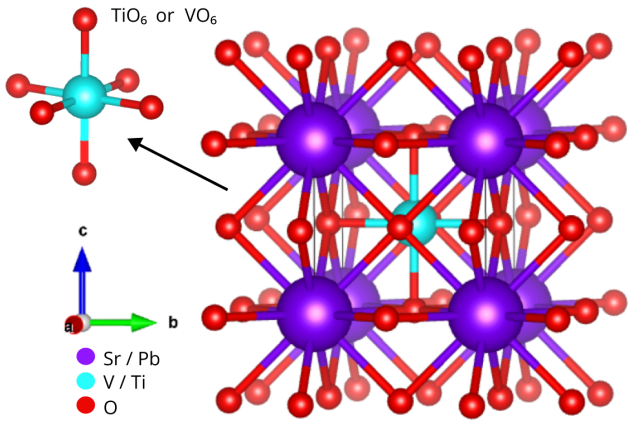


FIG. 1. Crystal structure of cubic perovskites $SrVO_3$ and $TiPbO_3$, showcasing the octahedral coordination of the transition metal (V or Ti) with oxygen ligands (O). The transition metal (V or Ti, light blue) is located at the center of an $MO_6$ octahedron (left inset), which forms the repeating structural unit of the perovskite lattice.

### B. Construction of Maximally Localized Wannier Functions

The electronic states within a solid are typically represented by Bloch states, which correspond to the eigenfunctions of the single-particle Hamiltonian for electrons in the periodic effective crystal potential. Since in this work we are employing density functional theory (DFT), the effective crystal potential in this case is represented by the Kohn-Sham potential, which consists of the electrostatic Coulomb potential generated by the nuclei, as well as the Hartree and exchange-correlation contributions due to electron-electron interactions. Bloch states $|\psi_{n\mathbf{k}}\rangle$ are characterized by a wave vector $\mathbf{k}$ within the first Brillouin zone (BZ) and a band index $n$. Wannier functions, on the other hand, can be a powerful tool in the study of the electronic and dielectric properties of materials: acting as the solid-state counterpart to "localized molecular orbitals" [9], they provide an insightful picture of the chemical bonding, which is instead missing from the Bloch picture of extended orbitals[10]. By transforming the occupied electronic manifold into a set of maximally localized Wannier functions (MLWFs), one gains deeper insights into chemical coordination and bonding characteristics. The most general operation that transforms the Bloch orbitals into a set of Wannier functions $|w_{\alpha\mathbf{R}}\rangle$ is given by:

$$|w_{\alpha\mathbf{R}}\rangle = \frac{V}{(2\pi)^3}\int_{\mathrm{BZ}} d^3k\, e^{-i\mathbf{k}\cdot\mathbf{R}} \sum_n U^{(\mathbf{k})}_{\alpha n}|\psi_{n\mathbf{k}}\rangle. \quad (1)$$

where $U^{(\mathbf{k})}$ unitary matrix that mixes the Bloch functions at the same $\mathbf{k}$-point. The Wannier orbitals are characterized by a unit cell index $\mathbf{R}$ and an additional index $\alpha$ that distinguishes different Wannier orbitals within the same unit cell. Since different choices for the $\mathbf{k}$-dependent unitary matrix $U^{(\mathbf{k})}$ lead to different Wannier orbitals (as per Equation 1), a unique set of Wannier functions can be obtained by imposing a "gauge" condition that minimizes the total quadratic spread $\Omega = \sum_\alpha \left(\langle r^2\rangle_\alpha - \langle \mathbf{r}\rangle^2_\alpha\right)$ of the Wannier orbitals. This approach results in the construction of "maximally localized Wannier functions" (MLWFs) [5].

## III. RESULTS & DISCUSSION

### A. Workflow

The process of extracting the crystal field splittings begins with the ionic relaxation of the conventional cell of $SrVO_3$ or $TiPbO_3$. This initial step optimizes the atomic positions within the unit cell to minimize the total energy, resulting in the ground-state geometry. Once the structure is relaxed, a self-consistent field (SCF) calculation is performed to obtain the ground-state Kohn-Sham energies and wavefunctions. The band structure is then calculated by tracing the Kohn-Sham eigenvalues along a predefined path connecting high-symmetry points in the Brillouin zone. The band structure will then serve as a guide for selecting the orbitals and the energy range that will be used to build the TB model. To identify the character of each band, we project the obtained band-structure onto specific orbitals, such as $s$, $p$, and $d$ orbitals. Based on these projections, initial guesses for the Wannier functions are selected to serve as the localized basis functions in the TB model. When building our model, we need to select by default the d orbitals of the 3d transition metal ion octahedrally coordinated with oxygen (namely either $V^{4+}$ or $Ti^{3+}$ in our case). Since both $SrVO_3$ and $TiPbO_3$ have one V or Ti ion octahedrally coordinated with oxygen in their conventional unit cell, this configuration results in a minimum of five $d$-orbital projectors, corresponding to the $d_{xy}$, $d_{yz}$, $d_{zx}$, $d_{x^2-y^2}$, and $d_{z^2}$ orbitals. Due to the non-uniqueness of Wannier functions[11], we use the VASP2WANNIER90 interface [12] to project the DFT Bloch states onto maximally localized Wannier functions (MLWFs) centered on the $d$-orbitals of the $V^{4+}$ and $Ti^{3+}$ ions. The Wannier90 code [13] is then employed to iteratively minimize the

spread functional, resulting in MLWFs centered on the $d$-bands of $V^{4+}$ (or $Ti^{3+}$). The Wannier90 code outputs the Hamiltonian in the Wannier basis, in which the Hamiltonian is non-diagonal. The matrix elements $h_{\alpha i,\beta j}$ in this basis correspond to hopping amplitudes for off-diagonal elements (i.e., when $i \neq j$) and to on-site energies for diagonal elements (i.e., when $i = j$). Specifically, the on-site energies of the $d$-centered Wannier functions can be found from the diagonal matrix elements where $i, j$ are the same atomic site, and $\alpha, \beta$ denote the $d$-orbitals [14]. Finally, the crystal field splitting $\Delta_o$ is calculated from the on-site energy difference between the $e_g$ orbitals ($d_{x^2-y^2}$ and $d_{z^2}$) and the $t_{2g}$ orbitals ($d_{xy}$, $d_{yz}$, and $d_{zx}$) of the octahedrally coordinated 3d transition metal, as follows:

$$\Delta_o = \frac{\left(\epsilon_{d_{x^2-y^2}} + \epsilon_{d_{z^2}}\right)}{2} - \frac{\left(\epsilon_{d_{xy}} + \epsilon_{d_{yz}} + \epsilon_{d_{zx}}\right)}{3} \qquad (2)$$

where each $\epsilon$ represents the on-site energy obtained from the Wannier-based TB Hamiltonian.

### B. $SrVO_3$

We first apply the workflow to derive the crystal field splitting in $SrVO_3$, a cubic perovskite where V is in the 4+ oxidation state with a $3d^1$ electron configuration. In this system, the $3d$ orbitals of $V^{4+}$ ions undergo octahedral crystal field splitting into lower-energy $t_{2g}$ and higher-energy $e_g$ orbitals due to interactions with the surrounding oxygen ligands [14]. The band structure of $SrVO_3$ (Fig. 2) shows distinct V-$d$ ($t_{2g}$ and $e_g$) and O-$p$ orbital bands, enabling an initial estimate of the crystal field splitting at approximately 2 eV. To quantify this numerically, we first construct MLWFs for only the $d$-orbital bands, confined to 4 eV to 11 eV relative to the Fermi energy. This model captures the full crystal field splitting of the V-$d$ states in $SrVO_3$. Next, we include the $p$-orbitals of oxygen, expanding the energy range to $-2$ eV to 11 eV. By constructing a tight-binding model that includes both V-$d$ and O-$p$ orbitals, we observe that the Wannier functions (WFs) centered on vanadium become significantly less extended, as seen in Table V in the Appenidx. The bonding and anti-bonding nature of the V-$d$ and O-2$p$ bands explains the localization trends. WFs from only anti-bonding bands are more extended due to retained O-$p$ character, as indicated by larger spreads (Table IV). However, if we expand the energy window to include both bonding and anti-bonding bands (and therefore increase the energy range and the number of WFs used in the tight binding model), the resulting WFs resemble atomic-like V and O functions more closely, and are therefore more localized. Athough there remains a small V-$d_{xy}$ component on the O sites to maintain orthogonality among WFs, this component is considerably reduced compared to when only the anti-bonding band is used [14]. For both sets, we record the on-site energies of the $V^{4+}$-centered $d$-like Wannier functions, which are tabulated in Table A of the Appendix. The crystal field splitting is then obtained as the difference of the mean V-$e_g$-like and V-$t_{2g}$-like Wannier function. When comparing the splitting of the on-site energies between the V-$e_g$-like and V-$t_{2g}$-like Wannier functions for the two sets (see Table I), it is evident that this splitting is reduced by 1.02 eV in the second set compared to the first. This reduction can be attributed to hybridization between the central V-$d$ orbitals and the $p$-orbitals of the surrounding oxygen ligands. In the first set, as previously mentioned, hybridization between the central V-$d$ orbitals and the $p$-orbitals of the surrounding oxygen ligands enforces significant O-$p$ character on the V-centered Wannier functions, which contributes to and increases the crystal field splitting value. We therefore conclude that the total $e_g$-$t_{2g}$ splitting of 2.69 eV obtained from the first set comprises significant V $d$ - O $p$ hybridization. However, since the 1.79 eV value for the crystal field splitting obtained from the 2nd set also likely includes contributions from V $d$-O$s$ hybridization, an even more comprehensive Wannier function construction would be needed to fully disentangle the various contributions to the crystal field splitting.

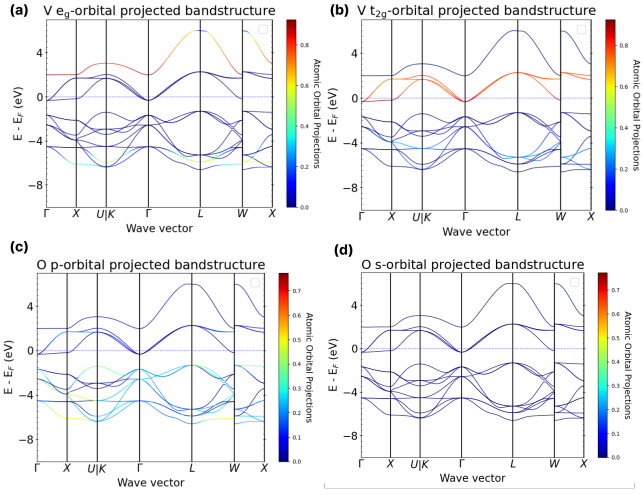


FIG. 2. Projected band structure of $SrVO_3$, illustrating the separation between $t_{2g}$ and $e_g$ states for the vanadium $d$-orbitals and the oxygen $p$-orbitals. Panel (a) V $t_{2g}$-orbital projected band structure, (b) V $e_g$-orbital projected band structure, (c) O $p$-orbital projected band structure, (d) O $s$-orbital projection. From Panel (d), we observe that none of the band in the displayed energy range has a predominant O$s$-orbital character. The Fermi Energy is found to be 4.7546 eV, and the energy bands are plotted with respect to it.

TABLE I. Crystal field splitting values for different bands included in the Wannier construction, with associated errors.

| **Bands used in WFs** | **Symbol** | **Value [eV]** | **Error [eV]** |
|---|---|---|---|
| only V-$d$ | $\epsilon_{e_g}^{(d)} - \epsilon_{t_{2g}}^{(d)}$ | 2.8099 | 0.0003 |
| V-$d$ and O-$p$ | $\epsilon_{e_g}^{(dp)} - \epsilon_{t_{2g}}^{(dp)}$ | 1.788 | 0.001 |

Finally, the accuracy of our TB model for $SrVO_3$ is validated by verifying that the atomic positions of the vanadium ions align with the $V^{4+}$-centered $d$-like Wannier functions, as seen from Table IV and V. Moreover, the WFs interpolated bandstructure is calculated using both sets of Wannier functions. We note that both sets of Wannier functions perform equally well in reconstructing the band structure within the energy range of 2 to 5 eV, where the $d$-orbitals of V dominate the electronic states, as seen from Figure 4.

### C. $TiPbO_3$

Similarly, we examine $TiPbO_3$, another cubic perovskite oxide, where Ti is in the 3+ oxidation state with a $3d^1$ configuration. The band structure of $TiPbO_3$, shown in Figure 3, reveals significantly mixed orbital character compared to $SrVO_3$. Unlike $SrVO_3$, which exhibits distinct $t_{2g}$ and $e_g$ bands, the bands in $TiPbO_3$ overlap considerably, reflecting probably a higher degree of hybridization of the d orbitals with the surrounding atoms. We follow a similar workflow as before. The first set of Wannier functions is constructed using 5 Ti-centered WFs, focusing on bands between 7 eV and 14 eV relative to the Fermi energy. For the second set, the energy range is expanded to $-1.8$ eV to 14 eV to include $p$-orbital-centered Wannier functions, adding 9 WFs corresponding to the three oxygen atoms in the unit cell. Finally, the energy range is extended further to $-11.6$ eV to 14 eV, incorporating $s$-orbital-centered Wannier functions for oxygen and resulting in a total of 17 WFs in the third set. As shown in Table II, the crystal field splitting decreases with the inclusion of oxygen $p$- and $s$-orbital-centered WFs, similar to the trend observed in $SrVO_3$. This reduction highlights the impact of hybridization on the crystal field splitting as derived from the first set of WFs, which reconstructs the $d$-orbital bands separately. Moreover, the smaller set of WFs again results in larger spreads, as seen by comparing Table VII with Table VIII and IX. However, we verify that, for all three sets, the $Ti^{3+}$-centered $d$-like Wannier functions have Cartesian coordinates matching those of the titanium ions, as expected. The interpolated band structure obtained from all three sets of WFs is reported in Figure 5 in the Appendix.

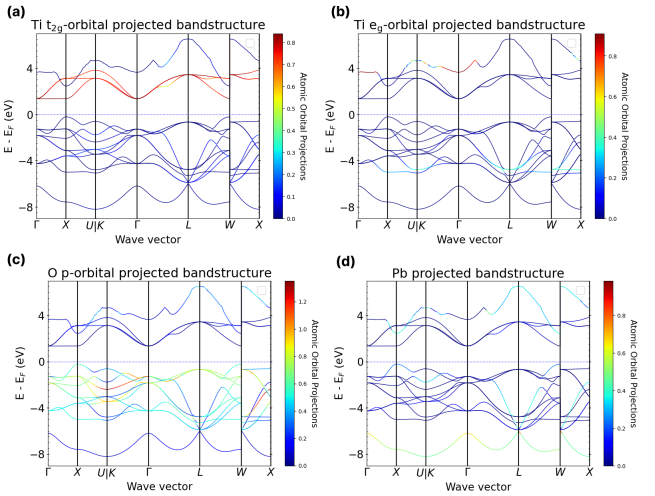


FIG. 3. Projected band structure of $TiPbO_3$ illustrating the orbital character contributions from different atomic species. (a) Ti $t_{2g}$-orbital projected band structure, (b) Ti $e_g$-orbital projected band structure, (c) O $p$-orbital projected band structure, and (d) Pb projected band structure. Unlike in $SrVO_3$, the bands in $TiPbO_3$ show significant orbital mixing, with no clear separation between the $t_{2g}$ and $e_g$ states. The Fermi Energy was found to be 6.17 eV, and the energy bands are plotted with respect to it.

TABLE II. Crystal field splitting values for different bands included in the Wannier construction, with associated errors

| **Bands used in WFs constr** | **Symbol** | **Value [eV]** | **Error [eV]** |
|---|---|---|---|
| only V-$d$ | $\epsilon_{e_g}^{(d)} - \epsilon_{t_{2g}}^{(d)}$ | 2.230 | 0.004 |
| V-$d$ and O-$p$ | $\epsilon_{e_g}^{(dp)} - \epsilon_{t_{2g}}^{(dp)}$ | 0.913 | 0.003 |
| V-$d$, O-$p$, and O-$s$ | $\epsilon_{e_g}^{(dps)} - \epsilon_{t_{2g}}^{(dps)}$ | 0.890 | 0.001 |

From Table II, we observe that using only Ti-$d$-centered Wannier functions, the crystal field splitting was found to be 2.230 eV. Including Ti-$d$ and O-$p$-orbitals reduced the splitting to 0.913 eV, while further inclusion of O-$s$-orbitals resulted in a slightly lower splitting of 0.890 eV. The lack of clear separation among the Ti $t_{2g}$, Ti $e_g$, and O $p$ bands in the band structure of $TiPbO_3$ indicates a greater degree of hybridization between the Ti $d$-orbitals and the oxygen $p$-orbitals in this system. This is further confirmed by the larger difference in crystal field splitting (greater than the 1.02 eV observed for $SrVO_3$) obtained when comparing the two distinct sets of Wannier functions: one constructed using only the bands with $3d$-orbital character and the other including oxygen orbitals.

## IV. METHODS

### Density functional theory calculations

The calculations for the electronic structure of $SrVO_3$ and $TiPbO_3$ have been carried out using DFT with the Projector Augmented Wave (PAW) method [15], as implemented in the Vienna ab initio Simulation Package [16–19] (VASP) version 5.4.4. The VASP-supplied PBE [20] PAW potentials version 5.4 were used, with the value of the valency of each atomic sphere being 10 for strontium, 5 for vanadium, 6 for oxygen, 12 for titanium, and 14 for lead. A plane wave kinetic energy cutoff of 550 eV was used, together with an electronic convergence threshold of $10^{-6}$ eV and a threshold of maximum force of any one ion of $10^{-2}$ eV Å$^{-1}$. The NSW parameter in VASP allowed for a maximum of 50 ionic steps for the system to relax into its ground state. The Brillouin zone was sampled using a Monkhorst-Pack mesh with a spacing of 0.02 Å$^{-1}$, and the width of the Gaussian smearing set to 0.01 eV. In all calculations, we employ non-spin-polarized DFT, as this approach is consistent with the fact that both $SrVO_3$ and $TiPbO_3$ are non-magnetic systems.

## V. SUMMARY & CONCLUSION

Using the combined capabilities of DFT and the MLWF formalism, we have investigated the crystal field splitting $\Delta_o$ for $V^{4+}$ in the octahedral environment of $VO_6$ in $SrVO_3$, and for $Ti^{3+}$ of $TiO_6$ in $TiPbO_3$. The crystal field splitting was determined by evaluating the on-site energies of the $d$-orbitals from a tight-binding (TB) model constructed with Maximally Localized Wannier Functions (MLWFs), which were designed to closely resemble the atomic $d$-orbitals of $V^{4+}$ and $Ti^{3+}$. For $SrVO_3$, constructing a tight-binding model using Wannier functions projected solely onto the $d$-orbitals yielded a crystal field splitting of 2.81 eV. Extending the TB model to include Wannier functions centered on the $p$-orbitals of oxygen resulted in overall more localized Wannier functions and a reduced crystal field splitting of 1.79 eV. This decrease demonstrates the significant contribution of hybridization with surrounding ligand $p$-orbitals to the ligand field in the previous derived value. In contrast, $TiPbO_3$ presents a more challenging case due to its mixed orbital character and lack of clear band separation. With only 5 Ti-$d$-centered Wannier functions (WFs), a crystal field splitting of 2.23 eV was obtained. Expanding the Wannier set to include oxygen $p$-orbital-centered WFs, the splitting decreased to 0.91 eV, and with the inclusion of both oxygen $p$- and $s$-orbital-centered WFs, it further reduced slightly to 0.89 eV. These results indicate that for $TiPbO_3$, 1.29 eV of the total crystal field splitting arises from $d$-$p$ hybridization, while 0.02 eV originates from $d$-$s$ hybridization. The larger reduction in the crystal field splitting for $TiPbO_3$ when enlarging the Wannier set compared to $SrVO_3$ suggests stronger $d$-oxygen ($p$ and $s$) hybridization in $TiPbO_3$. This aligns with the observation that the band structure of (Fig. 3) does not exhibit the clear separation of $t_{2g}$ and $e_g$ bands seen in $SrVO_3$). To completely isolate the pure electrostatic contribution to the crystal field splitting, a set of Wannier functions centered on all relevant orbitals would need to be computed. Lastly, we note that none of the constructed Wannier sets for $TiPbO_3$ yielded an interpolated band structure as closely resembling the DFT-computed band structure as achieved for $SrVO_3$. However, the bands with predominant O-$s$ and O-$p$ character were still well reproduced by the Wannier interpolated band structure (see Figure 5), indicating that the derived crystal field splitting values for $TiPbO_3$ can still be considered fairly accurate. Overall, this study demonstrates the capability of constructing tight-binding models with Wannier functions even for challenging systems like $TiPbO_3$, which exhibit poorly separated bands. It also highlights the importance of selecting an appropriate energy window and Wannier function set to construct a suitable TB model, which is essential for accurately deriving properties such as the crystal field splitting.

## ACKNOWLEDGMENTS

I acknowledge the computation time provided by the Quantum Matter Institute's computing cluster, as well as Professor Joerg Rottler at the University of British Columbia for granting access to the VASP license.

## Appendix A: Appendix

| | **Only V-$d$** | **V-$d$ + O-$p$** |
|---|---|---|
| $\epsilon_{d_{xy}}$ | 6.060837 | 4.895412 |
| $\epsilon_{d_{yz}}$ | 6.060826 | 4.895382 |
| $\epsilon_{d_{zx}}$ | 6.060827 | 4.895382 |
| **Mean** ($\varepsilon_{t_{2g}}$) | $6.06083 \pm 0.00001$ | $4.895392 \pm 0.00001$ |
| $\epsilon_{d_{x^2-y^2}}$ | 8.87040 | 6.681992 |
| $\epsilon_{d_{z^2}}$ | 8.87040 | 6.684025 |
| **Mean** ($\varepsilon_{e_g}$) | $8.8707115 \pm 0.0003$ | $6.6830085 \pm 0.001$ |

TABLE III. Comparison of on-site energies and crystal field splitting values for $V^{4+}$-centered $d$-like Wannier functions constructed using only 3$d$ orbitals versus including both 3$d$ and oxygen $p$ orbitals. The uncertainties for the $t_{2g}$ and $e_g$ mean values were calculated based on the standard deviation divided by the square root of the sample size (3 for $t_{2g}$ and 2 for $e_g$). Note: for the 2nd set, we are omitting the on-site energies of the 9 WFs centered on the p-orbitals of oxygen, as we are only interested in reporting the on-site energies of the $V^{4+}$-centered $d$-like Wannier functions.

| WF Number | Center Coordinates (Å) | Spread (Å$^2$) |
|---|---|---|
| 1 | (1.908129, 1.908129, 1.908129) | 3.29851247 |
| 2 | (1.908129, 1.908129, 1.908129) | 1.95264099 |
| 3 | (1.908129, 1.908129, 1.908129) | 1.95265841 |
| 4 | (1.908129, 1.908129, 1.908129) | 3.40400305 |
| 5 | (1.908129, 1.908129, 1.908129) | 1.95267656 |

TABLE IV. WF centers and spreads for vanadium-centered Wannier functions in $SrVO_3$, when we only include the d-orbitals of vanadium in the construction of the tight binding model.

| WF Number | Center Coordinates (Å) | Spread (Å) |
|---|---|---|
| 1 | (1.908067, 1.908129, 1.906649) | 1.27536288 |
| 2 | (1.908134, 1.908129, 1.908135) | 0.75179643 |
| 3 | (1.908129, 1.908129, 1.908142) | 0.75175883 |
| 4 | (1.907745, 1.908130, 1.908096) | 1.31876994 |
| 5 | (1.908141, 1.908129, 1.908129) | 0.75175691 |

TABLE V. WF centers and spreads for vanadium-centered Wannier functions in $SrVO_3$ when we include both the oxygen p orbitals in the construction of the tight-binding model.

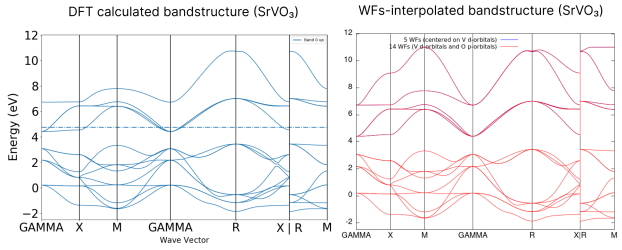


FIG. 4. Comparison of DFT computed bandstructure and reconstructed band structure of $SrVO_3$ using two different sets of Wannier functions (WFs). The blue lines represent the band structure reconstructed with 5 WFs centered on the V $d$-orbitals, while the red lines represent the reconstruction with 14 WFs, including both V $d$-orbitals and O $p$-orbitals. Although the inclusion of O $p$-orbitals in the Wannier construction (14 WFs) leads to a more accurate representation of the full electronic structure, the quality of the Wannier-interpolated band structure is very similar. We note that in the first set of Wannier functions, where MLWFs were constructed solely for the $d$-orbital bands, the interpolated band structure naturally reproduces only the $d$-band contributions.

| Quantity | Only Ti-$d$ | Ti-$d$ + O-$p$ |
|---|---|---|
| $\epsilon_{d_{xy}}$ | 9.589241 | 8.31594 |
| $\epsilon_{d_{yz}}$ | 9.58921 | 8.315581 |
| $\epsilon_{d_{zx}}$ | 9.583362 | 8.309073 |
| **Mean** ($E_{t_{2g}}$) | $9.587271 \pm 0.003$ | $8.313531333 \pm 0.003$ |
| $\epsilon_{d_{x^2-y^2}}$ | 11.899884 | 9.406448 |
| $\epsilon_{d_{z^2}}$ | 11.73462 | 9.04755 |
| **Mean** ($E_{e_g}$) | $11.817252 \pm 0.08$ | $9.226999 \pm 0.2$ |
| $\Delta_o$ | $2.229981 \pm 0.001$ | 0.913467667 |

TABLE VI. Comparison of on-site energies and crystal field splitting values for $Ti^{3+}$-centered $d$-like Wannier functions constructed using only $3d$ orbitals versus including both $3d$ and oxygen $p$ orbitals. Averages, associated uncertainties, and crystal field splitting values are shown.

| WF Number | Center Coordinates (Å) | Spread (Å$^2$) |
|---|---|---|
| 1 | (1.990002, 1.965455, 1.963597) | 15.56094260 |
| 2 | (1.960919, 1.960949, 1.960905) | 1.67887288 |
| 3 | (1.960903, 1.960921, 1.960912) | 1.68398896 |
| 4 | (1.941535, 1.952037, 1.965810) | 18.87839696 |
| 5 | (1.960920, 1.960955, 1.960918) | 1.67569860 |

TABLE VII. WF centers and spreads for vanadium-centered Wannier functions in $TiPbO_3$, when we only include the d-orbitals of titanium in the construction of the tight binding model.

| WF Number | Center Coordinates (Å) | Spread (Å$^2$) |
|---|---|---|
| 1 | (2.043523, 2.051313, 2.088552) | 8.20037992 |
| 2 | (1.960849, 1.961052, 1.960702) | 0.78445781 |
| 3 | (1.960981, 1.961029, 1.960914) | 0.78540027 |
| 4 | (1.939829, 1.947476, 2.053274) | 8.27652261 |
| 5 | (1.960853, 1.960899, 1.961115) | 0.79083593 |

TABLE VIII. WF centers and spreads for titanium-centered Wannier functions in $TiPbO_3$ when we include the d-orbitals of titanium and the oxygen p orbitals in the construction of the tight-binding model.

| WF Number | Center Coordinates (Å) | Spread (Å$^2$) |
|---|---|---|
| 1 | (2.028114, 2.045195, 2.045807) | 7.52136403 |
| 2 | (1.960855, 1.960985, 1.960740) | 0.77628239 |
| 3 | (1.960976, 1.961017, 1.960911) | 0.77800688 |
| 4 | (1.957077, 1.967631, 2.012641) | 7.44972837 |
| 5 | (1.960906, 1.960927, 1.961047) | 0.78254193 |

TABLE IX. WF centers and spreads for titanium-centered Wannier functions in $TiPbO_3$ when we include the d-orbitals of titanium and the oxygen s and p orbitals in the construction of the tight-binding model.

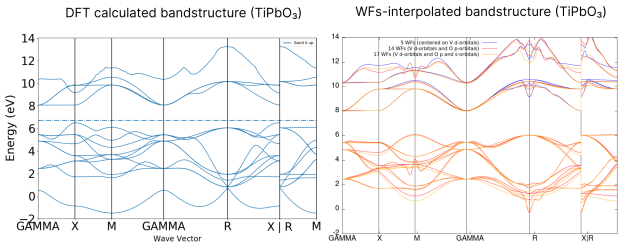


FIG. 5. Comparison of DFT computed bandstructure and reconstructed band structure of $TiPbO_3$ using three different sets of Wannier functions (WFs). The blue lines represent the band structure reconstructed with 5 WFs centered on the Ti *d*-orbitals, while the red lines represent the reconstruction with 14 WFs, including both Ti *d*-orbitals and O *p*-orbitals. The orange line represents the interpolated band structure using 17 WFs, including both Ti *d*-orbitals and O *p*-orbitals.
.


[1] J. S. Griffith, *The theory of transition-metal ions* (Cambridge university press, 1961).

[2] R. Schlapp and W. G. Penney, Influence of Crystalline Fields on the Susceptibilities of Salts of Paramagnetic Ions. II. The Iron Group, Especially Ni, Cr and Co, Physical Review **42**, 666 (1932).

[3] J. Adams, Bonding energy models, in *Encyclopedia of Materials: Science and Technology*, edited by K. J. Buschow, R. W. Cahn, M. C. Flemings, B. Ilschner, E. J. Kramer, S. Mahajan, and P. Veyssière (Elsevier, Oxford, 2001) pp. 763–767.

[4] N. Marzari, A. A. Mostofi, J. R. Yates, I. Souza, and D. Vanderbilt, Maximally localized wannier functions: Theory and applications, Rev. Mod. Phys. **84**, 1419 (2012).

[5] N. Marzari and D. Vanderbilt, Maximally localized generalized wannier functions for composite energy bands, Phys. Rev. B **56**, 12847 (1997).

[6] H. Bethe, Termaufspaltung in kristallen, Annalen der Physik **395**, 133 (1929).

[7] W. G. Penney and R. Schlapp, The influence of crystalline fields on the susceptibilities of salts of paramagnetic ions. i. the rare earths, especially pr and nd, Physical Review **41**, 194 (1932).

[8] W. G. Penney and R. Schlapp, The influence of crystalline fields on the susceptibilities of salts of paramagnetic ions. i. the rare earths, especially pr and nd, Phys. Rev. **41**, 194 (1932).

[9] S. F. Boys, Localized orbitals and localized adjustment functions, in *Quantum Theory of Atoms, Molecules, and the Solid State*, edited by P.-O. Löwdin (Academic Press, New York, 1966) pp. 253–262.

[10] S. Beck, A. Hampel, O. Parcollet, C. Ederer, and A. Georges, Charge self-consistent electronic structure calculations with dynamical mean-field theory using quantum espresso, wannier 90 and triqs, Journal of Physics: Condensed Matter **34**, 235601 (2022).

[11] P. Novák, K. Knížek, and J. Kuneš, Crystal field parameters with wannier functions: Application to rare-earth aluminates, Phys. Rev. B **87**, 205139 (2013).

[12] C. Franchini, R. Kováčik, M. Marsman, S. S. Murthy, J. He, C. Ederer, and G. Kresse, Maximally localized Wannier functions in $LaMnO_3$ within PBE+U, hybrid functionals and partially self-consistent GW: an efficient route to construct *ab-initio* tight-binding parameters for $e_g$ perovskites, Journal of Physics: Condensed Matter **24**, 235602 (2012).

[13] A. A. Mostofi, J. R. Yates, G. Pizzi, Y.-S. Lee, I. Souza, D. Vanderbilt, and N. Marzari, An updated version of wannier90: A tool for obtaining maximally-localised wannier functions, Computer Physics Communications **185**, 2309 (2014).

[14] A. Scaramucci, J. Ammann, N. A. Spaldin, and C. Ederer, On the calculation of crystal field parameters using wannier functions (2014), arXiv:1405.3804 [cond-mat.mtrl-sci].

[15] P. E. Blöchl, Projector augmented-wave method, Physical Review B **50**, 17953 (1994).

[16] G. Kresse and J. Hafner, Ab initio molecular dynamics for liquid metals, Physical Review B **47**, 558 (1993).

[17] G. Kresse and J. Hafner, Ab initio molecular-dynamics simulation of the liquid-metal–amorphous-semiconductor transition in germanium, Physical Review B **49**, 14251 (1994).

[18] G. Kresse and J. Furthmüller, Efficiency of ab-initio total energy calculations for metals and semiconductors using a plane-wave basis set, Computational Materials Science **6**, 15 (1996).

[19] G. Kresse and J. Furthmüller, Efficient iterative schemes for ab initio total-energy calculations using a plane-wave basis set, Physical Review B **54**, 11169 (1996).

[20] J. P. Perdew, K. Burke, and M. Ernzerhof, Generalized gradient approximation made simple, Phys. Rev. Lett. **77**, 3865 (1996).

[21] Y. Nomura and R. Akashi, Density functional theory, in *Encyclopedia of Condensed Matter Physics (Second Edition)*, edited by T. Chakraborty (Academic Press, Oxford, 2024) second edition ed., pp. 867–878.

[22] W. Kohn and L. J. Sham, Self-consistent equations including exchange and correlation effects, Physical review **140**, A1133 (1965).

[23] G. Kresse and D. Joubert, From ultrasoft pseudopotentials to the projector augmented-wave method, Phys. Rev. B **59**, 1758 (1999).

[24] P. E. Blöchl, Projector augmented-wave method, Phys. Rev. B **50**, 17953 (1994).

[25] J. P. Perdew, A. Ruzsinszky, G. I. Csonka, O. A. Vydrov, G. E. Scuseria, L. A. Constantin, X. Zhou, and K. Burke, Restoring the density-gradient expansion for exchange in solids and surfaces, Phys. Rev. Lett. **100**, 136406 (2008).

[26] Y.-S. Lee, M. B. Nardelli, and N. Marzari, Band structure and quantum conductance of nanostructures from maximally localized wannier functions: The case of functionalized carbon nanotubes, Phys. Rev. Lett. **95**, 076804 (2005).

[27] C. A. Morrison, Classical point-charge model, in *Angular Momentum Theory Applied to Interactions in Solids* (Springer Berlin Heidelberg, Berlin, Heidelberg, 1988) pp. 111–118.

[28] H. Bethe, Termaufspaltung in kristallen, Annalen der Physik **395**, 133 (1929).

[29] E. Rogers and P. Dorenbos, A comparison of the transition metal 3d1 crystal field splitting with the lanthanide 5d1 crystal field splitting in compounds, Journal of Luminescence **155**, 135 (2014).